Journal of
Materials Chemistry C

Materials for optical, magnetic and electronic devices

Accepted Manuscript

This article can be cited before page numbers have been issued, to do this please use: E. Carlos, S. Dellis, N. Kalfagiannis, L. Koutsokeras, D. Koutsogeorgis, R. Branquinho, R. Martins and E. Fortunato, *J. Mater. Chem. C*, 2020, DOI: 10.1039/D0TC01204A.

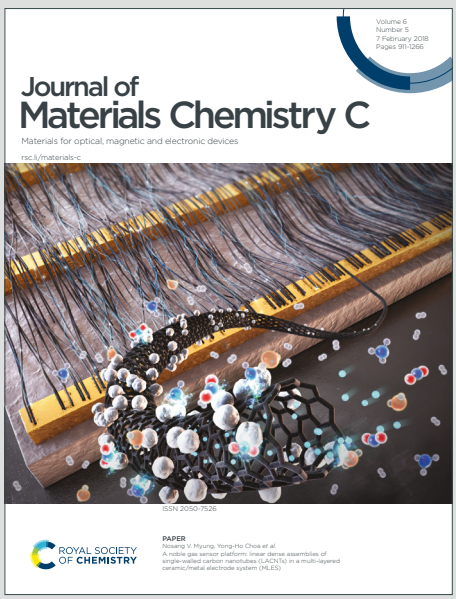

ROYAL SOCIETY OF CHEMISTRY

rsc.li/materials-c

View Article Online
DOI: 10.1039/D0TC01204A

Laser induced ultrafast combustion synthesis of solution-based AlO_x for thin film transistors

Emanuel Carlos[1,2], Spilios Dellis[2], Nikolaos Kalfagiannis[2], Loukas Koutsokeras[3], Demosthenes C. Koutsogeorgis[2], Rita Branquinho[1*], Rodrigo Martins[1] and Elvira Fortunato[1*]*

[1]CENIMAT/i3N Departamento de Ciência dos Materiais, Faculdade de Ciências e Tecnologia (FCT), Universidade NOVA de Lisboa (UNL), and CEMOP/UNINOVA, 2829-516 Caparica, Portugal.
[2]School of Science and Technology, Nottingham Trent University, Nottingham, NG11 8NS, UK.
[3]Cyprus University of Technology, Research Unit for Nanostructured Materials Systems, Kitiou Kyprianou 36, 3041, Lemesos, Cyprus

*E-mail: demosthenes.koutsogeorgis@ntu.ac.uk, ritasba@fct.unl.pt and emf@fct.unl.pt;

Abstract

Solution processing of amorphous metal oxides using excimer laser annealing (ELA) has been lately used as a viable option to implement large-area electronics, offering high quality materials at a reduced associated cost and process time. However, the research has been focused on semiconductor and transparent conductive oxide layers rather than on the insulator layer. In this work we present amorphous aluminum oxide (AlO_x) thin films produced at low temperature (≤150 °C) via combustion synthesis triggered by ELA, for oxide thin film transistors (TFTs) suitable for manufacturing flexible electronics. The study showed that combining ELA and combustion synthesis leads to an improvement in the dielectric thin film's densification in a shorter time (≤ 15 min). Optimized dielectric layers were obtained combining a short drying cycle at 150 °C followed by ELA treatment. High breakdown voltage ($4MV \cdot cm^{-1}$) and optimal dielectric constant (9) was attained. In general, TFT devices comprising the AlO_x fabricated with a drying cycle of 15 min followed by ELA presented great TFT properties, a high saturation mobility ($20.4 \pm 0.9\ cm^2 \cdot V^{-1} \cdot s^{-1}$), a small subthreshold slope ($0.10 \pm 0.01\ V \cdot dec^{-1}$) and a turn-on voltage ~0 V. ELA is shown to provide excellent quality solution-based high-κ AlO_x dielectric, that surpass other methods, like hot plate annealing and deep ultraviolet (DUV) curing. The results achieved are promising and expected to be of high value to the printed electronic industry due to the ultra-fast film densification and the surface/area selective nature of ELA.

Keywords: Low temperature processing, excimer laser annealing, solution combustion synthesis, oxide thin film transistors, solution based high-κ dielectric, printed electronics

View Article Online
DOI: 10.1039/D0TC01204A

1. INTRODUCTION

Over the last decade, solution-based metal oxide (MO) materials have become excellent candidates for thin film transistors (TFTs), offering conductors, semiconductors and high-κ dielectrics applicable to flexible and large area electronics.[1–6] Several processing techniques have been used to fabricate the constituent layers for the TFTs, like inkjet-printing, spray-coating, flexographic printing, screen printing, dip-coating and the most widely utilised spin-coating.[2,7–9] These techniques allow to reduce the associated fabrication costs (compared to vacuum technology) and at the same time can provide a high carrier mobility, excellent uniformity and operational stability. The high processing temperatures required to process most semiconductors and dielectric layers has been surpassed with the use of solution combustion synthesis (SCS) and deep-ultraviolet (DUV) photochemical activation. SCS provides additional thermal energy, via an exothermic reaction, resulting in a reduction of the external heating required (both in duration and temperature) for the film formation; i.e. the removal of organic solvents and film densification.[10,11] The DUV concurrent treatment additionally allows for the cleavage of alkoxy groups, active metals, and oxygen atoms to promote the metal-oxide-metal (M−O−M) network formation.[12–15] Overall, the combinatorial utilisation of SCS and DUV improves condensation and densification of the resultant metal oxide thin filmed, at processing temperatures ≤150 °C.[2,12,16–18] However, these methods require long processing times (≥ 30 min) that are not suitable for large-scale roll-to-roll (R2R) processes.[12,16,19] In a R2R processing line, annealing times are restricted by the length of the in-line curing ovens. For example, for a moderate web speed of 1 m/min and a typical oven length of 5 m, the curing time for each processed layer is limited to 5 min.[12,20,21]

Consequently, the industry demands alternative methods that can deliver a rapid annealing process.[22,23] Lately, excimer laser annealing (ELA) has been introduced as a favourable alternative in the fabrication of solution-based MO thin films. This method offers ultrafast

View Article Online
DOI: 10.1039/D0TC01204A

processing (in the nanosecond regime), with precise and selective energy delivery , both in depth via critical photon energy absorption as well as spatially (over a well-defined location), [24,25] resulting in a significant improvement of the electronic properties of MO thin films, that can outperform conventional annealing.[25,26] Nevertheless most effort has concentrated in semi-conductive and conductive thin films [23–32], with a notable lack of work on dielectric materials, despite its importance in the robust operation of TFTs.[18] Laser annealing of sol-gel processed HfO_2 has been reported by Teodorescu et al.[33] demonstrating the applicability of XeCl (308 nm) in the densification of amorphous hafnium oxide structure while achieving a high dielectric constant. However, a double coated layer was required (to eliminate nanoporosity, as well as a very high number of pulses (10000) and a 30 min annealing at 150 °C prior to ELA. Anodization is another promising solution process for the production of high quality dielectric thin films for application in TFTs.[34–38]

The promise of future state-of-the-art electronics (like wearable electronics) can only be enabled by low cost, easy to process, high quality dielectrics, that will allow low power consumption, as well as good mechanical and operational stability.[19,20,25] High-κ dielectric materials such as ZrO_2, HfO_2, Ta_2O_5, SrO_x, $ZrGdO_x$ or Al_2O_3 increase the areal capacitance of the gate dielectric allowing low operation voltage of TFTs.[2,39,40] Among these dielectrics, amorphous Al_2O_3 is one of the most promising due to its characteristic properties such as its high dielectric constant (~9) combined with a large band gap (8.9 eV), low interfacial trap density with semiconductors, high breakdown electric field.[18] At the same time, Al_2O_3 can be obtained from aluminium which is one of the most abundant materials on earth and hence it meets current demands for use of non-critical materials in the life-cycle assessment.[7]

In this work we demonstrate the production of amorphous aluminium oxide (AlO_x) thin films from solution and via a combination of SCS and ELA, and we report the performance of TFTs comprising these thin films. We applied a short drying cycle (15 min or 1 min) at low

View Article Online
DOI: 10.1039/D0TC01204A

temperature (≤150 °C) after spin coating of the solution. Subsequently the samples were irradiated with a few pulses (1 to 3) from a KrF (248 nm) excimer laser, varying the laser fluence. The dielectric quality of the AlO_x layers was evaluated via metal insulator semiconductor (MIS) devices, prior to implementing them in low operation voltage TFTs.

2. EXPERIMENTAL SECTION

2.1. Precursor solution preparation

Aluminum nitrate nonahydrate ($Al(NO_3)_3 \cdot 9H_2O$, Fluka, 98%) was dissolved in 2-methoxyethanol (2-ME, $C_3H_8O_2$, ACROS Organics, 99%), to yield a solution with an Al^{3+} ion concentration of 0.1 M. Urea ($CO(NH_2)_2$, Sigma, 98%) was then added to the prepared solution was maintained under constant stirring (430 rpm) for at least 1 h after dissolving the precursors. The urea to aluminum nitrate molar proportion was 2.5:1, to guarantee the redox stoichiometry of the reaction.[41] The precursor solution was filtered through a 0.20 μm hydrophilic filter before use.

2.2. Dielectric deposition, processing and characterization

Prior to deposition all substrates (p-type silicon wafers, of 1-10 Ω·cm, with size of 2.5cm×2.5 cm) were cleaned in an ultrasonic bath at 60 °C in acetone for 10 min, then in 2-isopropanol for 10 min and dried under nitrogen (N_2); followed by a 10 min UV/Ozone surface activation step in a PSD-UV Novascan system. Thin films were deposited by spin coating a single layer of the AlO_x precursor solution for 35 s at 2000 rpm (Laurell Technologies) followed immediately by a short drying cycle (hot plate annealing) at 150 °C with two different durations, 15 min or 1 min. Then, the photonic processing was performed, on different areas of the sample and with various laser conditions (fluence and number of pulses). The photonic processing station comprises a KrF excimer laser (Lambda Physik 305i, λ = 248 nm, 25 ns pulse duration) and a beam delivery system that provides the sample with a top hat profile laser spot (3x3 mm^2 in size) with fluence (energy density, mJ/cm^2) uniformity better than 2 % across the area of the

View Article Online
DOI: 10.1039/D0TC01204A

laser spot. The photonic processing station is described in detail elsewhere.[42,43] Finally, reference layers thermally annealed on a hotplate for 1h at 300 °C (without any photonic processing) were also fabricated, for comparison.

The films´ structure was assessed by glancing angle X-ray diffraction (GAXRD) performed on an X'Pert PRO PANalytical powder diffractometer using the Cu Kα line radiation (λ = 1.540598 Å) with an angle of incidence fixed at 0.9°. The surface morphology was investigated by atomic force microscopy (AFM, Asylum MFP3D). Spectroscopic ellipsometry measurements of the thin films deposited on silicon substrates were made over an energy range of 1.5−6.0 eV, at an incident angle of 70°, with a Jobin Yvon Uvisel system, in order to access the films´ thickness.

X-Ray Reflectivity (XRR) measurements were performed in a Rigaku Ultima IV diffractometer equipped with a multilayer X-ray mirror, using the Cu Ka line. The X-ray generator was operated at 40 kV and 40 mA and the reflected intensity was recorded by a scintillator detector in the range of 0.1 to 5 degrees 2 theta.

Fourier Transform Infra-Red (FTIR) spectroscopy characterization of the thin films was performed using an Attenuated Total Reflectance (ATR) sampling accessory (Smart iTR) equipped with a single bounce diamond crystal on a Thermo Nicolet 6700 Spectrometer. The spectra were acquired at a 45° incident angle in the range of 4500−540 cm^{-1} and with a 4 cm^{-1} resolution.

2.3. Electronic device fabrication and characterization

Two type of devices were fabricated for the evaluation of the quality of the AlO_x thin films produced: Metal-Insulator-Semiconductor (MIS) capacitors and Thin-Film-Transistor (TFTs).

MIS capacitors were produced by depositing an AlO_x single layer onto p-type silicon substrates as described above. Aluminum electrodes with an area of 7.85×10^{-3} cm^2 (dots of 1 mm in diameter 100 nm thickness), were deposited by thermal evaporation via a shadow mask on top

View Article Online
DOI: 10.1039/D0TC01204A

of the insulators, with similar but unpatterned aluminium electrodes being also deposited on the back of the silicon wafer (after removal of the native SiO_2 by scratching with a diamond tip pen). Electrical characterization was performed measuring both the capacitance−voltage and capacitance-frequency characteristics in the range of 1 kHz to 1 MHz, using a semiconductor parameter analyser (Keysight B1500A).

TFTs were produced in a staggered bottom-gate architecture, by depositing the single layer AlO_x onto p-type silicon substrates to act as gate dielectric.

The indium-gallium-zinc oxide (IGZO) semiconductor film (30 nm thick) was sputtered onto the dielectric thin film via a shadow mask. The deposition was performed using a commercial IGZO ceramic target (2:1:2 In:Ga:Zn atomic ratio) by RF magnetron sputtering in an Ar+O_2 (14 sccm and 2 sccm respectively) atmosphere and without intentional substrate heating in an AJA 1300-F system.[44]

Finally, source and drain aluminum electrodes (80 nm thick) were deposited by thermal evaporation via a shadow mask, forming TFTs with a channel length (L) of 90 μm and width (W) of 1000 μm, as shown in the inset of Figure 6 (a). Thereafter the IGZO TFTs were annealed at 150 °C, for 1 h in air. A back contact of 80 nm thick aluminum film was also deposited on the back of the silicon wafer to improve the ohmic contact.

The current−voltage characteristics of the devices were obtained in double sweep mode in ambient conditions using a semiconductor parameter analyser (Agilent 4155C) attached to a microprobe station (Cascade M150) inside a dark box.

The saturation mobility (μ_{SAT}) was determined in the saturation region of the $I_{DS}^{1/2}$ vs V_{GS} plot (with a linear fitting) from the following equation:

$$I_{DS} = \left(\frac{C_{ox} W \mu_{SAT}}{2L}\right)(V_{GS} - V_T)^2$$

View Article Online
DOI: 10.1039/D0TC01204A

where I_{DS} is the drain current, C_{ox} is the gate dielectric capacitance per unit area, L and W are the channel length and width respectively, V_{GS} is the gate voltage and V_T is the threshold voltage.

To assess device shelf life stability tests were performed after 1 year of storage in atmospheric conditions. Positive gate bias stress tests were performed on the TFTs using a semiconductor parameter analyzer (Keysight 4200SCS) and probe station (Janis ST-500) under atmospheric conditions by applying a constant gate voltage (corresponding to 0.5 MV/cm electric field) for one hour. The transfer characteristics were measured at fixed time intervals during the bias-stress process.

View Article Online
DOI: 10.1039/D0TC01204A

3. RESULTS AND DISCUSSION

The combinatorial methodology (SCS and ELA) implemented in this work, to achieve ultra-rapid high-quality solution-based M-O-M thin film formation, is depicted in Figure 1. At the outset, the metal precursor ($Al(NO_3)_3 \cdot 9H_2O$) is dissolved in 2-methoxyethanol (2-ME) and stirred for more than 12 h at room temperature (20–28 °C), where a ligand exchange reaction occurs from nitrate to hydroxide (Figure 1 (a)). Then the as-spun films are subjected to a short drying cycle (15 min or 1 min) at 150 °C (Figure 1 (b)). The choice of 150 °C, besides allowing the use of flexible substrates, was also made in order to sit roughly in the middle of the range defined by the boiling point of the solvent utilised (126 °C for 2-ME and hence some solvent removal is achieved), but below the threshold for combustion (180 °C and hence no combustion is initiated).[19]

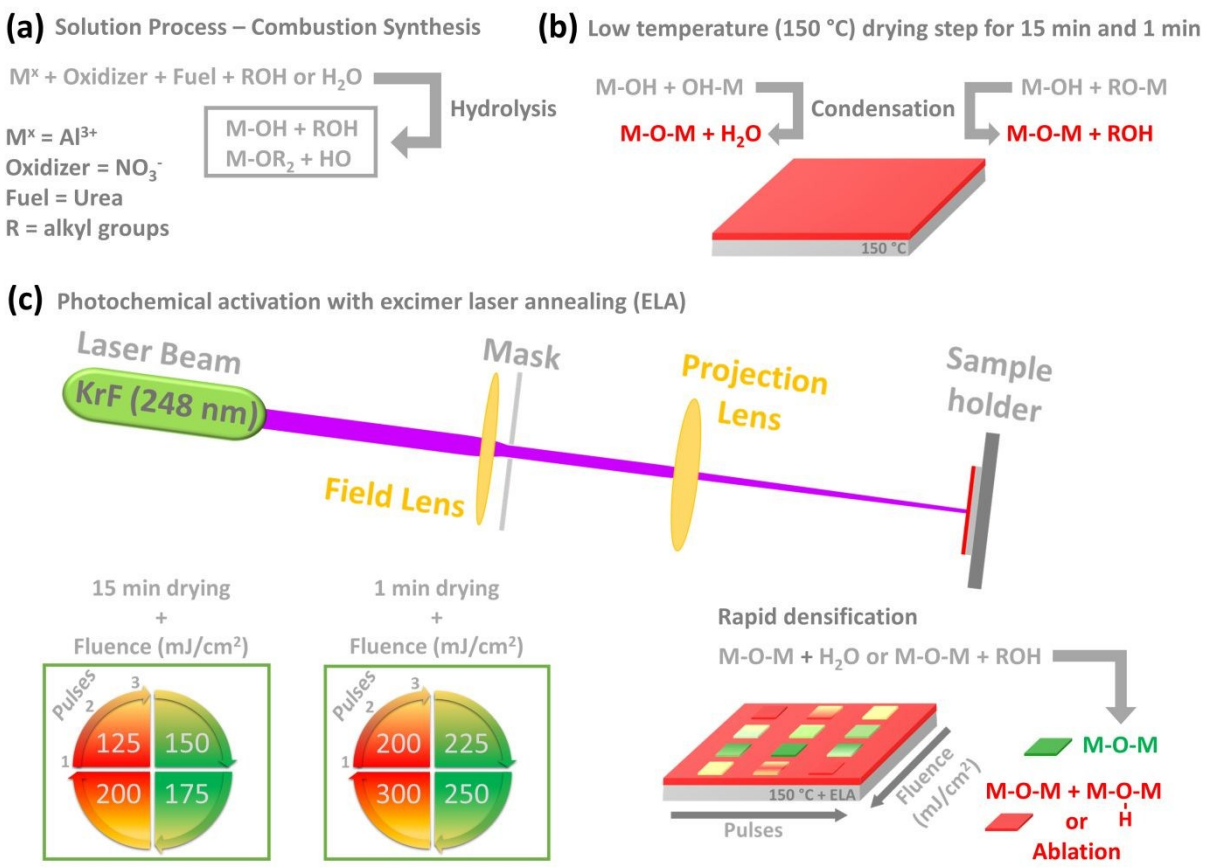

Figure 1. Illustration of the SCS and ELA combinatorial approach showing the (a) hydrolysis and (b) condensation mechanism of metal-oxide precursors; (c) Schematic representation of the

View Article Online
DOI: 10.1039/D0TC01204A

photonic processing for AlO_x thin films with different fluences and number of pulses, after 15 min or 1 min of hotplate drying at 150 °C immediately after spin coating.

Previous work[10] has revealed that the precursor solution displays an absorption peak well in the vicinity of a KrF excimer laser emission (248 nm). Naturally, this wavelength enables the photochemical cleavage of alkoxy groups, activating oxygen and metal ions, for the facilitation of the M-O-M network formation.[12] This solid-state chemical reaction is extremely fast and rapidly activates the reaction between the oxidizer (aluminium nitrate) and the fuel (urea). Additionally, the ultra-fast character of ELA enables the utilization of flexible substrates,[45] along with reducing the processing time drastically (as compared to DUV lamp irradiation typically requiring 30 min).[10] In Figure 1 (c), the circular schematics depict (in a clockwise manner) the increasing fluence and number of pulses applied on samples of each drying cycle. The coloured coded regions indicate AlO_x thin films obtained at different conditions. The colour intermixing suggests conditions where the photonic processing was either not enough to cause densification or was excessive and caused damage (red regions), and where it was suitable for the formation of AlO_x thin films (green regions).

3.1. Thin films structural characterization

The degree of densification can be revealed by the critical angle of an X-ray Reflectivity (XRR) measurement. Figure 2 (a) shows the XRR curves around the critical angle for 5 characteristic cases: the reference thin film (hotplate treated for 1h at 300 °C), the as spun film after drying at 150 °C for 15 min and for 1 min, as well as the same two dried films photonically processed with one laser pulse at 175 mJ/cm^2 and 250 mJ/cm^2 respectively. By qualitatively comparing the critical angles of the dried films, one can notice that both samples have the same critical angle and thus density, independently of the drying time. The additional photonic processing has resulted in a considerable densification compared to the dried thin films and notably present a similar density to the reference sample (1h at 300 °C). Therefore, it immediately educes that

View Article Online
DOI: 10.1039/D0TC01204A

the photonic processing approach can provide AlO_x thin films of similar density to those produced by a long duration higher temperature thermal (hotplate) annealing, but at a considerable fraction of the time and in a macroscopically cold process. The XRR curves were fitted with a three layer model (AlO_x film/SiO_2/Si) using Parrat's formalism.[46] The density extracted for the dried samples was 1.6 ± 0.1 g/cm^3, irrespective of the drying time. On the other hand, the density of the reference film was found to be 2.6 ± 0.1 g/cm^3, which is in agreement to values reported in the literature (~2.53 g/cm^3).[47] The photonically processed samples were found to have densities of 2.4 ± 0.1 g/cm^3 (for the 15 min + 175 mJ/cm^2) and 1.7 ± 0.1 g/cm^3 (for the 1 min + 250 mJ/cm^2) respectively.

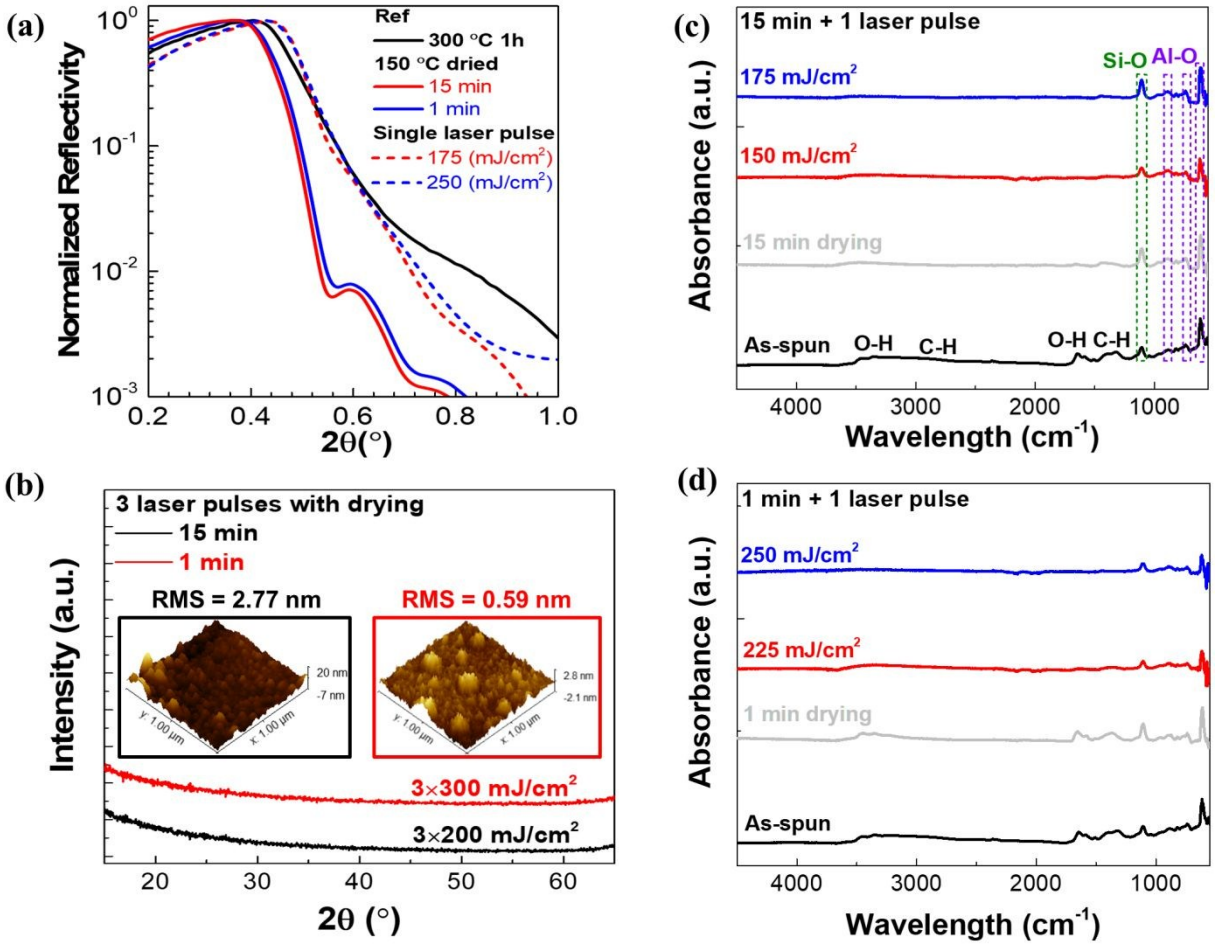

Figure 2. (a) XRR measurements of 5 selected samples showing the critical angle, (b) XRD diffractograms and AFM images (1×1 μm^2) of two samples dried at 15 min and 1 min, combined with photonic processing at the highest fluence values in each case (200 mJ/cm^2 and 300 mJ/cm^2 respectively) and maximum pulses (three pulses), (c) and (d) FTIR spectra of AlO_x thin films before and after single laser pulse photonic processing of the 15 min and 1 min dried (at 150 °C) sample respectively.

View Article Online
DOI: 10.1039/D0TC01204A

The microstructure of the solution-based AlO_x thin films was investigated by grazing angle X-ray diffraction (GAXRD). The absence of any diffraction peaks in Figure 2 (b) reveals that the thin films are amorphous, for both drying cycles combined with the photonic processing, even at the highest fluences and number of pulses. The insets in Figure 2 (b) are show the films' surface morphology obtained by atomic force microscopy (AFM) measurements for the highest fluences. A surface roughness ($\leq$ 2.8 nm) was observed for both drying cycles combined with photonic processing at the highest fluence and number of pulses. However, the surface morphology was not highly uniform, with some peak to valley values at 27.2 nm and 4.9 nm, for 15 min and 1 min drying cycle, respectively. For lower fluences the surface roughness was below 2 nm which guarantee a more uniform interface between the dielectric and the semiconductor.

In order to evaluate the extent of solvent removal, the AlO_x thin films were characterized by attenuated total reflection Fourier-transform infrared spectroscopy (ATR-FTIR), as shown in Figure 2 (c) and (d), for the two drying cycles respectively. All samples show an absorbance peak attributed to Si-O vibration (1107 cm^{-1}), due to the presence of native oxide on the Si wafer. Absorption bands related to O–H stretching vibrations (3700 – 3000 cm^{-1}; 1630 cm^{-1}; 1575 cm^{-1}) associated to water absorption and C–H (3090 – 2800 cm^{-1}; 1500 – 1300 cm^{-1}) due to the organic solvent, can be observed on the as-spun samples (prior to drying) and after both drying cycles at 150 °C (for both 15 or 1 min, prior to ELA). Evidently, the residuals are more prominent after the shorter drying cycle. A subsequent ELA treatment even with a single pulse seems to eliminate the residual solvent, as demonstrated by the diminishing relevant bands in the FTIR spectra, with increasing the laser fluence. For a full set of FTIR spectra for all the samples see Figure S1 and S2 in Supplementary Information. Finally, the absorption peaks observed at, 889, 739–748 and 611–601 cm^{-1}, are attributed to the presence of Al–O chemical bonds.[48]

View Article Online
DOI: 10.1039/D0TC01204A

3.2. Dielectric thin film electrical characterization

The electrical performance of the dielectric was evaluated by measuring the capacitance-voltage (C-V), capacitance-frequency (C-f) and breakdown field (E) of metal-insulator-semiconductor (MIS) structures. A summary of these results is shown in Figure 3, while the full measurements analytically can be found in Figures S3, S4, S5 and S6, as well as Tables S1 and S2 in the Supplementary Information. Each MIS device was replicated three times for reproducibility purposes.

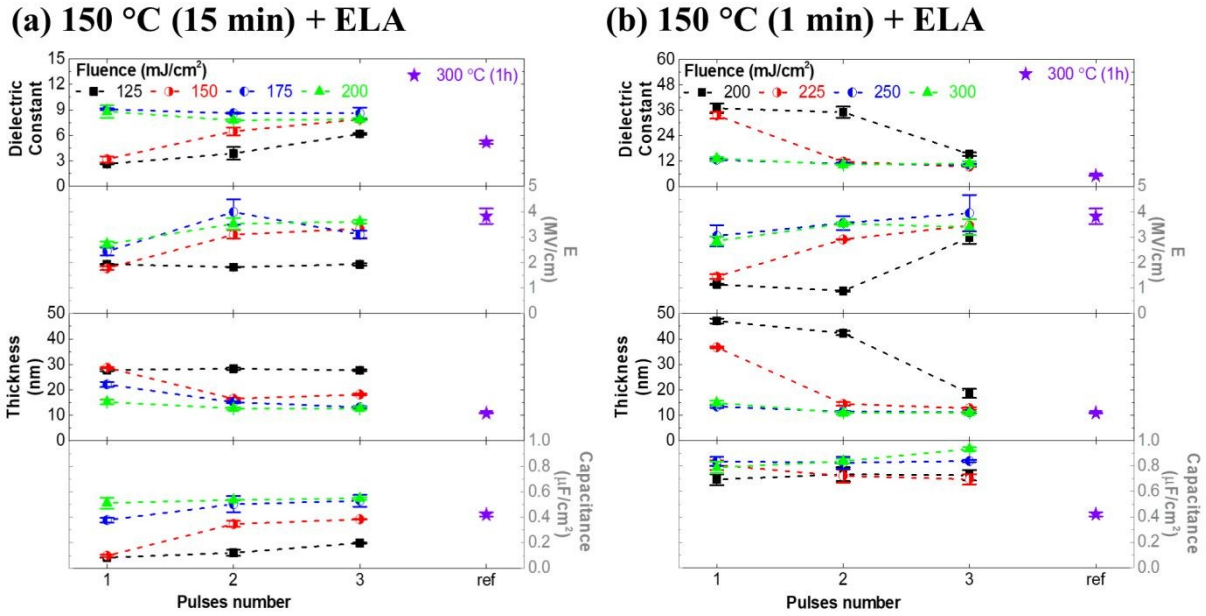

Figure 3. Statistical analysis of AlO_x thin films' performance: dielectric constant, breakdown voltage (E), thickness and capacitance measured at 1 kHz, for all fluences and number of pulses applied on films with initial drying of (a) 15 min and (b) 1 min. For comparison the equivalent characteristic of the reference device (thermally annealed at 300 °C for 1h) is also shown.

The films dried for 15 min (Figure 3a), show a considerable improvement of the dielectric constant as the fluence and the number of pulses is increased. For fluences above 150 mJ/cm^2, a dielectric constant of ~9 (calculated at 1 kHz) is achieved, which is typical for Al_2O_3 achieved via PVD techniques.[49] Interestingly, the dielectric constant of the reference MIS device (annealed at 300 °C for 1 h) was surpassed even with the lower fluence of 125 mJ/cm^2 using 3 pulses. These results corroborate the XRR findings, suggesting that ELA enhances condensation and densification of the AlO_x thin film, providing an improved dielectric constant

View Article Online
DOI: 10.1039/D0TC01204A

in an ultra-rapid fashion and at lower processing temperatures. Conversely when the drying cycle is shorter (1min, Figure 3b), higher fluences were required in order to achieve reasonable values for the dielectric constant. The unrealistic values (>10) for the dielectric constant achieved at lower fluences are explained by the presence of ionic movement (see Figure S4 in Supplementary Information).

Another important factor is the durability and stability of the AlO_x dielectric thin films, as expressed by the breakdown voltage. ELA provided films with breakdown voltages up to 4.0 MV/cm, closely matching the breakdown voltage demonstrated by the reference sample (3.8 MV/cm). The breakdown voltage values were found to show a local maximum within the range of fluences investigated, therefore the optimum annealing conditions have been identified. These are two pulses of 175 mJ/cm^2 and three pulses of 250 mJ/cm^2 for the 15 min and 1 min drying cycles respectively, presenting breakdown voltages of 4.0 ± 0.5 MV/cm and 3.9 ± 0.7 MV/cm, whilst the reference device presented a breakdown voltage of 3.82 ± 0.03 MV/cm. The thickness required in order to calculate the breakdown voltage and the dielectric constant, was determined by UV-VIS ellipsometry, for each device. Besides Figure 3, the full results for all devices fabricated can be seen in the Supplementary Information in Tables S1 and S2 as well as Figures S5 and S6.

The devices' aerial capacitance values at 1 kHz are shown in the bottom panel of Figure 3 (a) and (b) for the two drying cycles. The majority of the ELA devices present a higher aerial capacitance than the reference device (0.42 ± 0.02 μF/cm^2). Full C-V characteristic curves at 100 kHz and a summary of aerial capacitance vs frequency is presented in the Supplementary Information in Figures S3 and S4, respectively. The drying cycles result in a considerable difference in the dispersive character of capacitance, with the shorter drying cycle being more adversely impacted (i.e. more dispersive) potentially due to the probable incomplete conversion and removal of the precursor.

View Article Online
DOI: 10.1039/D0TC01204A

In conclusion, the combination of short drying cycles (15 or 1 min) at relatively low temperatures (150 °C) and ELA delivers in an ultra-fast manner AlO_x thin films with similar or enhanced dielectric properties compared to those achieved via high temperature (300 °C) prolonged (1h) thermal annealing.

3.3. Low operation voltage IGZO/AlO_x TFTs

Informed by the results presented above (namely the dielectric constant and breakdown voltage) a suitable selection of AlO_x thin films were tested in TFT devices, with IGZO as the semiconductor. A summary of the electrical characteristics of these devices is shown in Figure 4 (a) and (b). The full set of the respective transfer curves for each device is shown in Figures S7 and S8 of the Supplementary Information. Device performance was assessed through the measurement of the hysteresis (V_{Hyst}), turn-on voltage (V_{ON} , the on-set voltage at which the drain current starts to increase), drain current on−off ratio (I_{ON}/I_{OFF}), subthreshold slope (SS), and saturation mobility (μ_{SAT}) which was calculated using the dielectric capacitance measured in AlO_x MIS devices at a frequency of 1 kHz (see Table S3 and S4 in Supplementary Information).

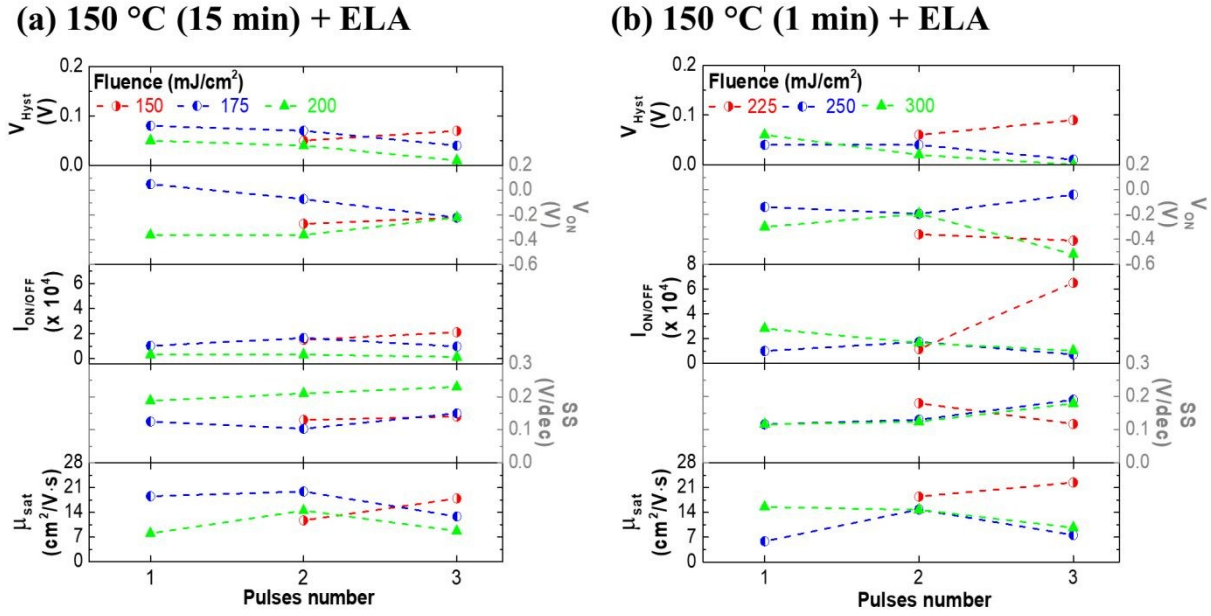

Figure 4. TFT parameters: hysteresis (V_{Hyst}), turn-on voltage (V_{ON}), current on-off ratio ($I_{ON/OFF}$), subthreshold slope (SS) and saturation mobility (μ_{SAT}), for the two drying cycles: (a) 15 min and (b) 1 min followed by ELA treatment.

View Article Online
DOI: 10.1039/D0TC01204A

All the devices exhibited low hysteresis (less than 0.15 V). A moderate hysteresis reduction with the increase of number of pulses and fluence was observed. Equally all of the device presented a current on-off ration of the order of 10^4. In the case of the 15 min drying cycle followed by ELA, the turn-on voltage presents an optimum value (closer to 0 V) at a fluence of 175 mJ/cm^2, whereas higher fluences and number of pulses result in a negative turn-on voltage. Below this optimum fluence some ionic species could remain in the dielectric, whereas above surface damage may occur compromising the quality of the semiconductor-dielectric interface. This is further supported by the deterioration of both the subthreshold slope and the saturation mobility. Surface damage and high density of generated defects is likely at higher fluences, since the solution combustion synthesis (SCS) is an exothermic reaction that occurs in the thin film in an ultra-rapid fashion (due to the ELA pulse lasting only a few nanoseconds). In the case of the 1 min drying cycle followed by ELA, a similar trend was found with an optimum fluence value of 250 mJ/cm^2. The results above are summarised in Figure 5 (a) were the best performing ELA devices, for each drying cycle, are presented alongside the reference device (300 °C for 1h).

.

View Article Online
DOI: 10.1039/D0TC01204A

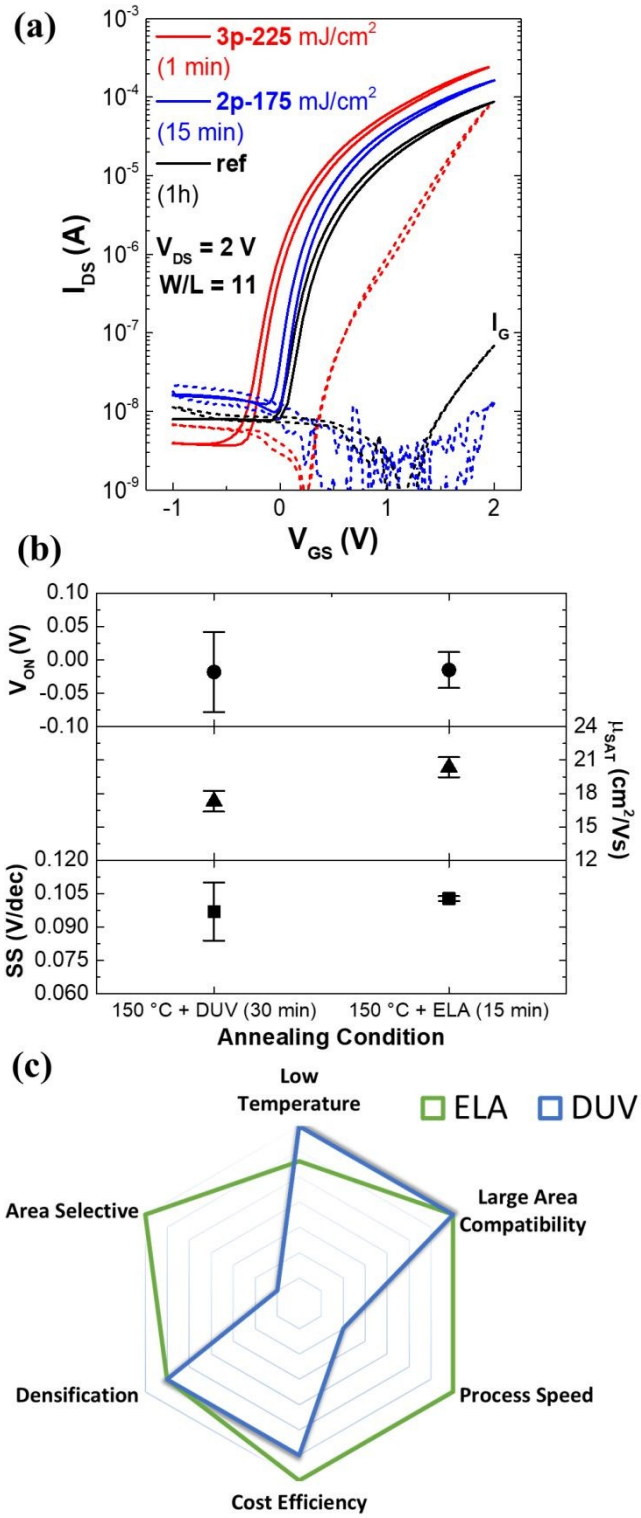

Figure 5. (a) Transfer characteristics of IGZO TFT devices fabricated with solution-based aluminium oxide (AlO_x) insulator thin films for different drying times (15 min and 1 min) followed by ELA treatment. The reference device (300 °C for 1h) is also shown for comparison. (b) Summary of TFT device characteristics using deep ultraviolet (DUV) for 30 min (previous report[10]) and this work using the 15 min drying followed by ELA. (c) Comparison of quality characteristics between ELA and DUV treatment for the production of solution-based oxides for the printed electronics industry.

View Article Online
DOI: 10.1039/D0TC01204A

Both drying cycles provide TFTs with comparable or better properties than the reference device, however, the 1 min drying followed by ELA present a higher gate leakage current. Furthermore, we present a comparison of the best performing ELA device (15 min drying cycle and 2x175 mJ/cm^2) to devices with AlO_x fabricated with DUV curing at low temperature[10] (the IGZO layer is identical in both cases). Figure 5 (b) shows a statistical analysis revealing that ELA provides solution processed AlO_x dielectric thin films for TFTs with similar electrical characteristics to the DUV devices, but with an improved saturation mobility (see also Table S5 in Supplementary Information). In general, we can conclude that the combination of ELA treatment with a short drying cycle, immediately after spin coating, can result in AlO_x thin films with quality comparable, if not better, than the standard approach of high temperature thermal annealing (hot plate). The implications of this approach are considerable for the industry of flexible and plastic electronics, as it lends itself to R2R production, for a variety of reasons including: - it enables the use of plastic substrates (maximum processing temperature 150 °C) as it is a macroscopically cold process; - it is rapid enough to allow inline processing while maintaining a reasonable web speed; - it is area selective via laser writing, removing the need for extra fabrication steps for patterning; - it offers oxide thin films of high quality from solution based materials. As such, this approach could provide a significant boost to the printed electronics industry. In comparison to DUV curing (see Figure 5(c)) ELA presents similarly high performance in densification and in large area processability but offers increased overall efficiency through its excellent area selectivity and its massively faster processing time as can be seen in the Supplementary Information in Table S6. The temperature rise in the metal oxide material is far more extreme with ELA, but at the same time considerably faster, resulting in a completely macroscopically cold process, unlike DUV processing. To investigate the effect of the ambient atmosphere on the IGZO/AlO_x TFTs were performed some ageing and stress measurements as depicted in Figure 6.

View Article Online
DOI: 10.1039/D0TC01204A

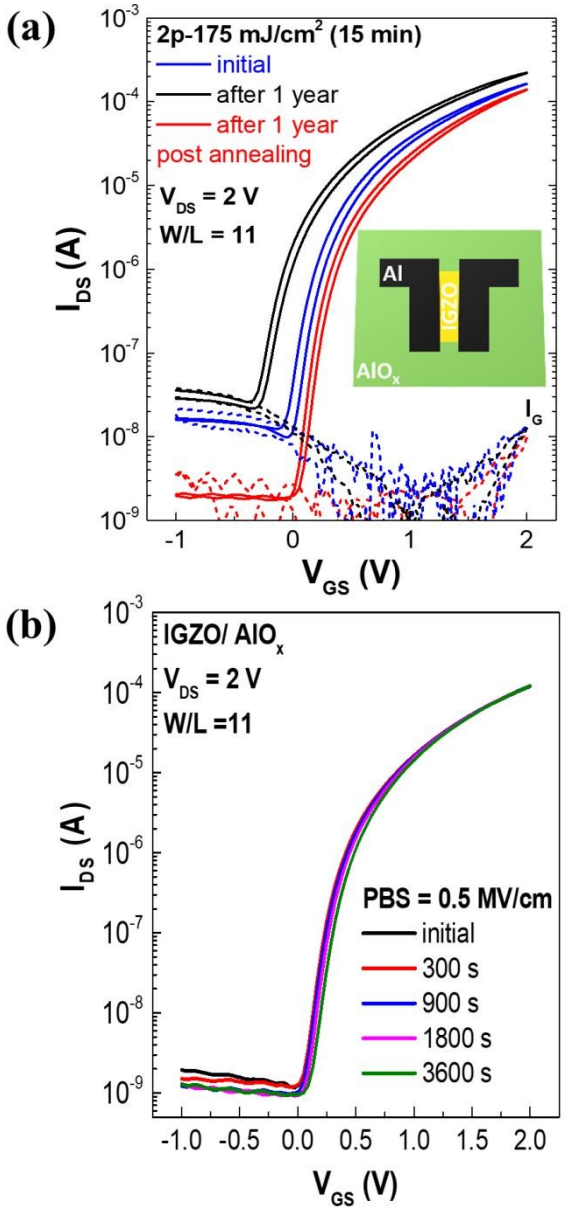

Figure 6. Stability tests for the best condition achieved with ELA treatment: (a) Ageing effects of IGZO/AlO_x TFTs after 1 year exposed in air environment without passivation and after a post annealing at 120 °C; inset shows the top view TFT schematic (each electrode had an area of 11.9 × 10^{-3} cm^2). (b) Positive gate-bias stress (PBS) measurements of 0.5 MV/cm on IGZO/AlO_x TFTs for 1 h in air environment.

Figure 6 (a) shows transfer characteristics of the same device taken a few days after full fabrication and after 1 year of storage in atmospheric conditions, to determine device ageing. In general, the device performance was preserved, however the turn-on voltage displayed a slight negative shift a year later, most probably associated to the increase of carrier density.[50] Also, a small increase of off-current was observed, most probably due to the humidity present

View Article Online
DOI: 10.1039/D0TC01204A

in atmospheric environment (which can be surpassed by device passivation).[51,52] To determine the device behaviour after one year but without the influence of surface adsorption of water molecules, a post annealing at 120 °C (30 min) was performed. As expected, the device´s on voltage recovered fully and furthermore the off current was improved by an order of magnitude compared to the initial fabrication. Following this, the device was subjected to a positive gate-bias stress (PBS) of 0.5 MV/cm for 3600 s as depicted in Figure 6 (b). The IGZO/AlO_x TFTs under PBS remained stable showing only a slight threshold voltage shift to a positive value of just 0.02 V, meaning that a reduced quantity of trap sites exists in the dielectric/semiconductor interface. As no deterioration was observed in the subthreshold slope under bias stress, the mechanism present is the charge trapping model.[53] Optimization of production parameters is ongoing, nonetheless these tests already prove the potential of ELA treatment for solution-based oxide TFTs.

View Article Online
DOI: 10.1039/D0TC01204A

4. CONCLUSIONS

In conclusion we have demonstrated the combustion solution synthesis alliance with ELA of AlO_x dielectric thin films at low temperatures in a short drying cycle (15 min or 1 min) and their implementation in TFTs. The AlO_x dielectric films revealed an amorphous nature, low roughness, high-κ (9), low leakage currents (10^{-6} A/cm^2 at 1 MV/cm) and high breakdown voltages ~4 MV/cm. These results indicate that ELA treatment is a viable platform for the fabrication of metal-oxide dielectric thin films at low processing temperatures. Subsequently ELA treatment in combination with combustion synthesis, can be the answer to obtain high performance printed metal oxide TFTs in the R2R industry.

View Article Online
DOI: 10.1039/D0TC01204A

ACKNOWLEDGEMENTS

This work is funded by FEDER funds through the COMPETE 2020 Programme and National Funds through FCT - Portuguese Foundation for Science and Technology under project number POCI-01-0145-FEDER-007688, Reference UID/CTM/50025. European Community H2020 NMP-22-2015 project 1D-NEON Grant Agreement 685758. E. Carlos acknowledges FCT-MCTES for a doctoral grant (Grant SFRH/BD/116047/2016) and IDS-FunMat-INNO project FPA2016/EIT/EIT RawMaterials Grant Agreement 15015. E. Fortunato acknowledges the ERC AdG grant 787410 from the project DIGISMART.

AUTHOR CONTRIBUTIONS

E.C., S.D., N.K., D.C.K. and R.B designed and planned the project. E.C., S.D. and N.K. fabricated and characterised the samples. L.K. performed the XRR measurements and analysis. E.C., D.C.K and R.B. analysed the data, prepared the figures and wrote the paper. All authors discussed the results and commented on the manuscript.

COMPETING INTERESTS

The Authors declare no Competing Financial or Non-Financial Interest.

SUPPLEMENTARY INFORMATION

The Supplementary Information contains the full data sets related to the production of AlO_x dielectric thin films from solution, by excimer laser annealing (ELA) treatment inducing combustion synthesis, and their application in thin film transistors (TFTs). Table S1 and S2 shows the statistical parameters of dielectric properties obtained from MIS devices. Figure S1 and S2 depicts FTIR spectra for all ELA conditions and for both drying durations, 15 min and

View Article Online
DOI: 10.1039/D0TC01204A

1 min, respectively. Figure S3, S4 and S5-S6 show the capacitance–voltage, capacitance–frequency and breakdown voltage (E) characteristics of Al/p-type Si/(AlOx)/Al MIS capacitors for both drying durations. Tables S3 and S4 depicts the electrical characteristics summary obtained from IGZO TFTs comprising the sol-gel AlO_x fabricated by all the different ELA treatments, while Figures S7 and S8 show the transfer curves of the same IGZO TFTs devices. Finally, Figure S9 depicts the typical output curves of two test TFT devices and the reference. Table S5 shows the statistical TFT parameters from a previous report using deep ultraviolet (DUV) curing for 30 min[10], alongside those of the optimum devices produced in this work (using the 15 min drying cycle followed by ELA). Table S6 depicts relevant low temperature solution-based AlO_x layers processed by different curing methods applied in TFTs reported previously in the literature.

DATA AVAILABILITY

The authors declare that all data supporting the findings of this study are available within the paper and its supplementary information files.

View Article Online
DOI: 10.1039/D0TC01204A

REFERENCES

1 M. Lorenz, M. S. Ramachandra Rao, T. Venkatesan, E. Fortunato, P. Barquinha, R. Branquinho, D. Salgueiro, R. Martins, E. Carlos, A. Liu, F. K. Shan, M. Grundmann, H. Boschker, J. Mukherjee, M. Priyadarshini, N. DasGupta, D. J. Rogers, F. H. Teherani, E. V Sandana, P. Bove, K. Rietwyk, A. Zaban, A. Veziridis, A. Weidenkaff, M. Muralidhar, M. Murakami, S. Abel, J. Fompeyrine, J. Zuniga-Perez, R. Ramesh, N. A. Spaldin, S. Ostanin, V. Borisov, I. Mertig, V. Lazenka, G. Srinivasan, W. Prellier, M. Uchida, M. Kawasaki, R. Pentcheva, P. Gegenwart, F. Miletto Granozio, J. Fontcuberta and N. Pryds, *J. Phys. D. Appl. Phys.*, 2016, **49**, 433001.

2 S. Park, C.-H. Kim, W.-J. Lee, S. Sung and M.-H. Yoon, *Mater. Sci. Eng. R Reports*, 2017, **114**, 1–22.

3 E. Fortunato, P. Barquinha and R. Martins, *Adv. Mater.*, 2012, **24**, 2945–2986.

4 M. Coll, J. Fontcuberta, M. Althammer, M. Bibes, H. Boschker, A. Calleja, G. Cheng, M. Cuoco, R. Dittmann, B. Dkhil, I. El Baggari, M. Fanciulli, I. Fina, E. Fortunato, C. Frontera, S. Fujita, V. Garcia, S. T. B. Goennenwein, C.-G. Granqvist, J. Grollier, R. Gross, A. Hagfeldt, G. Herranz, K. Hono, E. Houwman, M. Huijben, A. Kalaboukhov, D. J. Keeble, G. Koster, L. F. Kourkoutis, J. Levy, M. Lira-Cantu, J. L. MacManus-Driscoll, J. Mannhart, R. Martins, S. Menzel, T. Mikolajick, M. Napari, M. D. Nguyen, G. Niklasson, C. Paillard, S. Panigrahi, G. Rijnders, F. Sánchez, P. Sanchis, S. Sanna, D. G. Schlom, U. Schroeder, K. M. Shen, A. Siemon, M. Spreitzer, H. Sukegawa, R. Tamayo, J. van den Brink, N. Pryds and F. M. Granozio, *Appl. Surf. Sci.*, 2019, **482**, 1–93.

5 K. K. Banger, Y. Yamashita, K. Mori, R. L. Peterson, T. Leedham, J. Rickard and H. Sirringhaus, *Nat. Mater.*, 2011, **10**, 45–50.

6 E. Yarali, C. Koutsiaki, H. Faber, K. Tetzner, E. Yengel, P. Patsalas, N. Kalfagiannis, D. C. Koutsogeorgis and T. D. Anthopoulos, *Adv. Funct. Mater.*, 2019, **1906022**, 1906022.

7 C. Glynn and C. O'Dwyer, *Adv. Mater. Interfaces*, 2017, **4**, 1600610.

8 W.-J. Lee, W.-T. Park, S. Park, S. Sung, Y.-Y. Noh and M.-H. Yoon, *Adv. Mater.*, 2015, **27**, 5043–5048.

9 J. Leppäniemi, O.-H. H. Huttunen, H. Majumdar and A. Alastalo, *Adv. Mater.*, 2015, **27**, 7168–7175.

10 E. Carlos, R. Branquinho, A. Kiazadeh, J. Martins, P. Barquinha, R. Martins and E. Fortunato, *ACS Appl. Mater. Interfaces*, 2017, **9**, 40428–40437.

11 E. Carlos, R. Martins, E. M. C. Fortunato and R. Branquinho, *Chem. – A Eur. J.*, 2020, chem.202000678.

12 Y.-H. Kim, J.-S. Heo, T.-H. Kim, S. Park, M.-H. Yoon, J. Kim, M. S. Oh, G.-R. Yi, Y.-Y. Noh and S. K. Park, *Nature*, 2012, **489**, 128–132.

13 D. Chae, J. Kim, J. Shin, W. H. Lee and S. Ko, *Curr. Appl. Phys.*, 2019, **19**, 954–960.

14 I. Bretos, R. Jiménez, J. Ricote and M. L. Calzada, *Chem. Soc. Rev.*, 2018, **47**, 291–308.

15 J.-W. Jo, Y.-H. Kim, J. Park, J. S. Heo, S. Hwang, W.-J. Lee, M.-H. Yoon, M.-G. Kim and S. K. Park, *ACS Appl. Mater. Interfaces*, 2017, **9**, 35114–35124.

16 M.-G. Kim, M. G. Kanatzidis, A. Facchetti and T. J. Marks, *Nat. Mater.*, 2011, **10**, 382–388.

17 S. K. Park, K.-H. K. T. K. H. K.-T. Kim, J.-W. W. Jo, S. Sung, K.-H. K. T. K. H. K.-T. Kim, W.-J. J. Lee, J. Kim, H. J. Kim, G.-R. R. Yi, Y.-H. H. Kim, M.-H. H. Yoon and S. K. Park, *Adv. Funct. Mater.*, 2015, **25**, 2807–2815.

18 E. Carlos, R. Branquinho, A. Kiazadeh, P. Barquinha, R. Martins and E. Fortunato,

View Article Online
DOI: 10.1039/D0TC01204A

ACS Appl. Mater. Interfaces, 2016, **8**, 31100–31108.

19 E. Carlos, J. Leppäniemi, A. Sneck, A. Alastalo, J. Deuermeier, R. Branquinho, R. Martins and E. Fortunato, *Adv. Electron. Mater.*, 2020, **6**, 1901071.

20 J. S. Chang, A. F. Facchetti and R. Reuss, *IEEE J. Emerg. Sel. Top. Circuits Syst.*, 2017, **7**, 7–26.

21 J. Leppäniemi, K. Ojanperä, T. Kololuoma, O.-H. Huttunen, J. Dahl, M. Tuominen, P. Laukkanen, H. Majumdar and A. Alastalo, *Appl. Phys. Lett.*, 2014, **105**, 113514.

22 S. K. Garlapati, J. S. Gebauer, S. Dehm, M. Bruns, M. Winterer, H. Hahn and S. Dasgupta, *Adv. Electron. Mater.*, 2017, **3**, 1–6.

23 Y.-H. Yang, S. S. Yang and K.-S. Chou, *IEEE Electron Device Lett.*, 2010, **31**, 969–971.

24 C. Y. Tsay and T. T. Huang, *Mater. Chem. Phys.*, 2013, **140**, 365–372.

25 S. Dellis, I. Isakov, N. Kalfagiannis, T. D. Anthopoulos, D. C. Koutsogeorgis, K. Tetzner, T. D. Anthopoulos and D. C. Koutsogeorgis, *J. Mater. Chem. C*, 2017, **5**, 2–6.

26 C. Chen, G. Chen, H. Yang, G. Zhang, D. Hu, H. Chen and T. Guo, *J. Mater. Chem. C*, 2017, **5**, 9273–9280.

27 Y.-H. Yang, S. S. Yang and K.-S. Chou, *J. Soc. Inf. Disp.*, 2011, **19**, 247.

28 J. Lee, S. Song, S. Cho, M. Song, Y. Kim, J. Kwon and M. Han, *IEE*, 2012, 135–138.

29 Q. Nian, M. Callahan, M. Saei, D. Look, H. Efstathiadis, J. Bailey and G. J. Cheng, *Sci. Rep.*, 2015, **5**, 1–12.

30 C. N. Chen and J. J. Huang, *J. Appl. Res. Technol.*, 2015, **13**, 170–176.

31 H. Huang, H. Hu, J. Zhu and T. Guo, *J. Electron. Mater.*, 2017, **46**, 4497–4502.

32 T. Nakajima, K. Shinoda and T. Tsuchiya, *Chem. Soc. Rev.*, 2014, **43**, 2027–2041.

33 V. S. Teodorescu, A. V. Maraloiu, M.-G. Blanchin, T. Yamada, C. S. Sandu, P. Delaporte and M. Zaharescu, in *CAS 2013 (International Semiconductor Conference)*, IEEE, 2013, vol. 1, pp. 77–80.

34 L. Lan and J. Peng, *IEEE Trans. Electron Devices*, 2011, **58**, 1452–1455.

35 W. Cai, S. Park, J. Zhang, J. Wilson, Y. Li, Q. Xin, L. Majewski and A. Song, *IEEE Electron Device Lett.*, 2018, **39**, 375–378.

36 T. C. Gomes, D. Kumar, L. Fugikawa-Santos, N. Alves and J. Kettle, *ACS Comb. Sci.*, 2019, **21**, 370–379.

37 S. Sagar, N. Mohammadian, S. Park, L. A. Majewski and B. C. Das, *Nanotechnology*, , DOI:10.1088/1361-6528/ab7fd1.

38 L. Xie, Y. Shao, X. Xiao, L. Zhang, X. Bi and S. Zhang, in *2014 21st International Workshop on Active-Matrix Flatpanel Displays and Devices (AM-FPD)*, IEEE, 2014, vol. 1, pp. 101–103.

39 C. Fan, A. Liu, Y. Meng, Z. Guo, G. Liu and F. Shan, *IEEE Trans. Electron Devices*, 2017, **64**, 4137–4143.

40 L. Zhu, G. He, W. Li, B. Yang, E. Fortunato and R. Martins, *Adv. Electron. Mater.*, 2018, **4**, 1800100.

41 R. Branquinho, D. Salgueiro, L. Santos, P. Barquinha, L. Pereira, R. Martins and E. Fortunato, *ACS Appl. Mater. Interfaces*, 2014, **6**, 19592–19599.

42 N. Kalfagiannis, A. Siozios, D. V. Bellas, D. Toliopoulos, L. Bowen, N. Pliatsikas, W. M. Cranton, C. Kosmidis, D. C. Koutsogeorgis, E. Lidorikis and P. Patsalas, *Nanoscale*, 2016, **8**, 8236–8244.

43 N. Kalfagiannis, D. C. Koutsogeorgis, E. Lidorikis and P. Patsalas, in *Nanoplasmonics - Fundamentals and Applications*, InTech, 2017, vol. i, p. 13.

44 A. Kiazadeh, H. L. Gomes, P. Barquinha, J. Martins, A. Rovisco, J. V. Pinto, R. Martins and E. Fortunato, *Appl. Phys. Lett.*, 2016, **109**, 051606.

45 A. Siozios, N. Kalfagiannis, D. V. Bellas, C. Bazioti, G. P. Dimitrakopulos, G.

View Article Online
DOI: 10.1039/D0TC01204A

Vourlias, W. M. Cranton, E. Lidorikis, D. C. Koutsogeorgis and P. Patsalas, *Nanotechnology*, 2015, **26**, 155301.

46 L. G. Parratt, *Phys. Rev.*, 1954, **95**, 359–369.

47 S. W. Smith, W. Wang, D. A. Keszler and J. F. Conley, *J. Vac. Sci. Technol. A Vacuum, Surfaces, Film.*, 2014, **32**, 041501.

48 J. M. Reyes, B. M. Perez Ramos, C. Z. Islas, W. C. Arriaga, P. R. Quintero and a. T. Jacome, *J. Electrochem. Soc.*, 2013, **160**, B201–B206.

49 J. Acharya, J. Wilt, B. Liu and J. Wu, *ACS Appl. Mater. Interfaces*, 2018, **10**, 3112–3120.

50 Y. Song, A. Katsman, A. L. Butcher, D. C. Paine and A. Zaslavsky, *Solid. State. Electron.*, 2017, **136**, 43–50.

51 J. S. Park, J. K. Jeong, H. J. Chung, Y. G. Mo and H. D. Kim, *Appl. Phys. Lett.*, 2008, **92**, 90–93.

52 S. W. Cho, D. E. Kim, K. S. Kim, S. H. Jung and H. K. Cho, *J. Mater. Chem. C*, 2017, **5**, 10498–10508.

53 T.-C. Chen, T.-C. Chang, T.-Y. Hsieh, W.-S. Lu, F.-Y. Jian, C.-T. Tsai, S.-Y. Huang and C.-S. Lin, *Appl. Phys. Lett.*, 2011, **99**, 022104.

View Article Online
DOI: 10.1039/D0TC01204A

Table of Contents/Abstract Graphic (max 20 words)

Excimer laser annealing (ELA) combined with combustion synthesis leads to high quality metal oxide TFTs in a short processing time.